Green Chemistry

Accepted Manuscript

ROYAL SOCIETY OF CHEMISTRY

www.rsc.org/greenchem

Green Chemistry

ARTICLE

Catalytic transfer hydrogenation of biomass-derived 5-hydroxymethyl furfural to the building block 2,5-bishydroxymethyl furan†

xReceived 00th January 20xx,
Accepted 00th January 20xx

DOI: 10.1039/x0xx00000x

www.rsc.org/

Weiwei Hao[a], Weifeng Li[a], Xing Tang[a], Xianhai Zeng[a], Yong Suna,[b,]*, Shijie Liu[c], and Lu Lin[a,]*

An efficient process for the catalytic transfer hydrogenation of biomass-derived 5-hydroxymethyl furfural (HMF) to 2,5-bishydroxymethyl furan (BHMF) was presented using ethanol as a hydrogen donor and solvent over low-cost $ZrO(OH)_2$. A HMF conversion of 94.1% and a DHMF selectivity of 88.9% were achieved at 423 K in 2.5 h. The fresh, spent, and regenerated catalysts were characterized comprehensively, and the OH group of $ZrO(OH)_2$ as sites for ligand exchange with ethanol was considered to be important for the activity.

Introduction

The depleting fossil-based resources alongside environmental deterioration have raised the concerns of sustainability of our society, economy, and environment. Abundant and inexpensive biomass, which is the only current renewable carbon source on earth, has attracted the increasing attention of worldwide people. Biorefinery concept is an important approach to address the increasing demand of energy and chemical building blocks for a wide range of applications, which may gradually alleviate the current dependence on fossil fuel resources.[1-3] The conversion of biomass materials to platform chemicals, such as 5-hydroxymethyl furfural (HMF)[4], levulinic acid (LA)[5, 6], furfural[7] and γ-valerolactone (GVL)[8], is the key step to realize this attractive prospect. These platform molecules retain moderate functionalities to ensure the required stability for storage and transportation and the essential reactivity for the upgrading to other chemicals and fuels compared to carbohydrates.[9, 10] Among these platform molecules, HMF, the so-called 'sleep giant', has been hailed as an important building block due to its rich chemistry and potential availability.[3, 11] Both the oxidation and reduction of HMF offer access to numerous valuable building blcoks, which include 2,5-furandicarboxylic acid (FDCA)[12, 13], 2,5-diformylfuran (DFF)[14, 15], 2,5-bishydroxymethyl furan (BHMF). A typical synthetic transformation is the selective reduction of the formyl group in HMF to yield BHMF that has a significant market potential for the production of resins, polymers, artificial fibers and crown ethers.[16-18]

However, only a few studies focused on the selective hydrogenation of HMF to BHMF because HMF can be converted to over-hydrogenated products of 2,5-dihydroxymethyltetrahydrofuran (DHMTF) and 2,5-dimethylfuran (DMF) easily in a conventional hydrogenation system which consists of noble metal catalysts and molecular H_2.[19-22] It is highly expensive for noble metal catalysts and the management of molecular H_2. Recently, the Cannizzaro reaction was applied to the conversion of HMF to BHMF, but an equimolar by-product was also formed by the oxidation of HMF.[23, 24] In addition, the selective hydrogenation of HMF to BHMF was also catalyzed by the Shvo catalyst and a high BHMF yield was obtained; however, the Shvo catalyst is expensive and hard to be recycled after reaction.[25]

Recently, multiple H_2-free catalytic systems have been presented and provide a better alternative for the hydro-upgrading of biomass-derived molecules. For example, Lobo and Vlachos reported that HMF can be hydrogenated to DMF with a high yield using 2-propanol as a hydrogen source over Ru/C.[26] The catalytic transfer hydrogenation (CTH) of LA and its esters to GVL by Meerwein–Ponndorf–Verley (MPV) reduction was also reported using alcohols as the hydrogen source and metal oxides/hydroxides as the catalysts.[27, 28] In addition, methanol was employed as an in situ hydrogen source for the hydrogenation of biomass-derived molecules.[29-31] These external H_2-free processes are cost-efficient because the use of noble metal and external molecular H_2 is avoided. Unit operations are also minimized by eliminating the introduction of external molecular H_2. Moreover, H donors such as methanol or ethanol are sustainable as these alcohols can be produced from renewable biomass resources.[32]

In this paper, we present a H_2-independent process for the selective hydrogenation of HMF to BHMF by MPV

[a] College of Energy, Xiamen University, Xiamen 361005, China.; sunyong@xmu.edu.cn; lulin@xmu.edu.cn.
[b] Key Laboratory of Biomass Energy and Materials of Jiangsu Province, Nanjing 210042, China.
[c] College of Environmental Science and Forestry, State University of New York, 1 Forestry Drive, Syracuse, NY 13210, USA.
† Electronic Supplementary Information (ESI) available: [details of any supplementary information available should be included here]. See DOI: 10.1039/x0xx00000x

reduction, in which low-cost ethanol and $ZrO(OH)_2$ are used as a H donor and a catalyst, respectively. MPV reduction has an exclusive selectivity to the hydrogenation of the carbonyl group; therefore, over-hydrogenated products like DHMTF and DMF would not become a concern in this study. The effects of different process parameters on the selectivity of products were investigated and a detailed characterization of the fresh and used catalysts was conducted. Finally, based on the results of the poisoning experiments, a plausible mechanism for the CTH of HMF to BHMF via MPV reduction over metal hydroxides was proposed.

Results and discussion

CTH of HMF into BHMF catalyzed by various metal hydroxides

Table 1 CTH of HMF into BHMF catalyzed by various metal hydroxides [a]

Entry	Catalyst	X, %	S_{BHMF}, %
1	$ZrO(OH)_2$	70.0	87.7
2	$Al(OH)_3$	21.0	58.8
3	$Ti(OH)_4$	28.5	18.7
4	$La(OH)_3$	21.0	24.2
5	$Sn(OH)_4$	52.1	-
6	$Mg(OH)_2$	-	-

[a] Reaction conditions: 1 g HMF, 0.5 g catalyst, 39 g ethanol, 423 K, 2h, and N_2 at atmospheric conditions.

Inexpensive metal hydroxides were employed as the catalysts for the CTH of HMF to BHMF in near-critical ethanol at 423 K for 2 h. HMF conversion and BHMF selectivity were highly dependent on the catalysts used. In the presence of $Mg(OH)_2$ as strong basic catalyst, the conversion of HMF and the yield of BHMF were negligible (Table 1, entry 6). When $Al(OH)_3$, $Ti(OH)_4$ or $La(OH)_3$ was used as the catalysts, HMF conversion was improved to a certain degree but still no greater than 30%, and the selectivities of BHMF of 18.7-58.8% were observed (Table 1, entries 2-4). Unexpectedly, a high HMF conversion of 70.0% with a BHMF selectivity of 87.7% was obtained if $ZrO(OH)_2$ was used as the catalyst under the same reaction conditions (Table 1, entry 1). When $Sn(OH)_4$ was employed, electronegativity (a key factor to strength and type of acid or base site of metal oxide) of which was equal to Zr^{4+}, HMF conversion reached 52.1%, however, BHMF yield was negligible (Table 1, entry 5). Meanwhile, 5-(hydroxymethyl)-furfural diethyl acetal (HMFDEA), 5-(ethoxymethyl)-furfural (EMF) and 5-(ethoxymethyl)-furfural diethyl acetal (EMFDEA) were detected shown in Table S1, which were synthesized by the acetalization and etherification of HMF with ethanol. Obviously, $ZrO(OH)_2$ as a typical acid-base catalyst (Scheme 2), which has appropriate electronegativity and the steric hindrance, was much more effective for the CTH of HMF to BHMF via MPV reduction compared to other metal hydroxides. Therefore, $ZrO(OH)_2$ was selected as the preferred catalyst for the subsequent experiments.

Reaction pathway for the conversion of HMF in ethanol

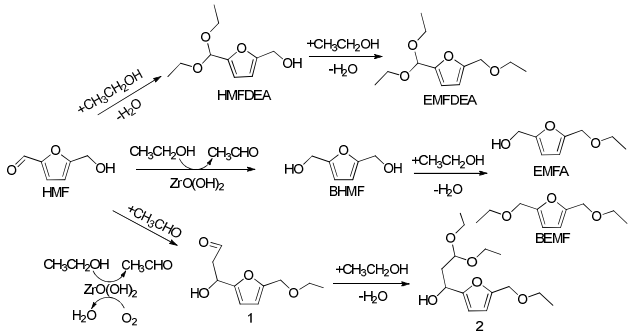

Scheme 1 Reaction pathway for the CTH of HMF in ethanol

As BHMF selectivity below 100% rendered from Table 1, it is obviously indicated that side reactions occurred during the CTH of HMF to BHMF. The main by-products in ethanol were deduced based on the results of GC-MS, and the reaction pathway is being elucidated in Scheme 1. Besides the desired product BHMF, a minute amounts of 5-(Ethoxymethyl)furfuryl alcohol (EMFA) and 2,5-bis(ethoxymethyl)furan (BEMF) were also detected, which are formed by the etherification of BHMF with ethanol. Recently, EMFA and BEMF were particularly attractive owing to their high energy densities and advantageous fuel blending properties. For instance, BEMF has been assessed as a diesel additive in a six-cylinder heavy duty engine. The European Stationary Cycle test was performed and revealed that no significant difference in engine operation was observed for all tested blending ratios. [33, 34] Moreover, a small amounts of HMFDEA and EMFDEA were also detected which were produced by acetal reaction of HMF followed by etherification in ethanol. The product distribution obtained is consistent with the reaction network, proposed by Jennifer D. Lewis et al., for the coupled transfer hydrogenation and etherification of HMF. [35] GC-MS spectra of the products were given in Figs.S1-10.

Effect of reaction temperature, reaction time and catalyst loading

When the reaction temperature was 383 K, a HMF conversion of only 26.8% was obtained, and selectivity of BHMF and HMFBEA 85.3% and 11.4% were achieved, respectively (Table 2, entry 1). An increase of temperature promoted HMF conversion and suppressed HMFDEA formation. If the temperature was up to 423 K, a HMF conversion of 70.0% was achieved, and the selectivity to BHMF was 87.7% (Table 2, entry 3). If the temperature was further increased to 463 K, HMF conversion was correspondingly improved to 98.9%, whereas the selectivity of BHMF dropped significantly down to 63.8% (Table 2, entry 5). However, the EMFA selectivity was obviously increased to 24.7% compared with that less than 3% when temperature was below 423 K, which illustrated that

high temperature significantly facilitated the etherification of BHMF with ethanol. Hence, a moderate reaction temperature of 423 K was selected for the subsequent studies.

The conversion of HMF was increased from 53.5% to 76.1% with the prolonging reaction time from 1 to 3 h (Table 2, entries 6-10). The BHMF selectivity was maintained about 87% even after a reaction time of 2.5 h (Table 2, entries 6-9). However, a slight decrease in the BHMF selectivity was obtained if the reaction time was prolonged to 3 h (Table 2, entry 10). An increase in the selectivity of EMFA indicated that the loss of BHMF selectivity was attributed mainly to the etherification of BHMF. Furthermore, the selectivity of HMFDEA was slightly decreased under the identical reaction conditions (Table 2, entry 10).

Table 2 The effect of reaction temperature, reaction time and catalyst loading on the CTH of HMF into BHMF. [a]

Entry	T, K	*t*, h	Catalyst, g	*X*, %	S_{BHMF}, %	S_{EMFA}, %	S_{HMFDEA}, %
1	383	2	0.5	26.8	85.3	0.0	11.4
2	403	2	0.5	39.5	88.6	0.0	7.1
3	423	2	0.5	70.0	87.7	2.6	6.4
4	443	2	0.5	91.5	81.6	10.1	2.8
5	463	2	0.5	98.9	63.8	24.7	1.1
6	423	1	0.5	53.8	87.5	2.1	6.7
7	423	1.5	0.5	59.6	87.8	2.6	5.8
8	423	2	0.5	70.0	87.7	2.6	6.4
9	423	2.5	0.5	72.4	86.9	3.9	5.7
10	423	3	0.5	76.1	83.9	8.3	4.3
11	423	2.5	0.25	48.0	84.4	1.8	11.1
12	423	2.5	0.5	72.4	86.9	3.9	5.7
13	423	2.5	0.75	88.5	89.8	2.8	2.2
14	423	2.5	1	94.1	88.9	1.8	1.0
15 [b]	423	2.5	1	89.4	86.2 (44) [c]	4.2	3.3

[a] Reaction conditions: 1 g HMF, 39 g ethanol, N_2 at atmospheric conditions.
[b] Using a crude HMF as substrate and reaction conditions for HMF synthesis: fructose, 1g; SiO_2@$AlCl_3$·$6H_2O$@ChCl, 1.7 g; MIBK, 40 mL; 373 K, 4h; the HMF yield is 55%.
[c] BHMF yield based on fructose.

If 0.25 g $ZrO(OH)_2$ was used, the HMF conversion of 48.0% and BHMF selectivity of 84.4% were obtained at 423 K in 2.5 h (Table 2, entry 11). An increase of catalyst loading from 0.25 to 1 g led to a remarkable increase of the HMF conversion to 94.1% (Table 2, entry 14). Meanwhile, a significant drop in the HMFDEA selectivity from 11.1% to 1.0% and a slight increase in the BHMF selectivity from 84.4 to 88.9% were observed (Table 2, entries 11-14).

In addition to pure HMF, a crude HMF from fructose [36] was also used for the synthesis of BHMF. First, a mixture of fructose, catalyst and MIBK was introduced to a flask and heated to 373 K with stirring. After a desired reaction time, the reaction mixture was cooled down to room temperature. The reaction product containing HMF was analyzed by GC to determine the HMF yield (55%), and then MIBK was recovered by vacuum distillation to obtain a crude HMF product. Eventually, the crude HMF with ethanol reacted over $ZrO(OH)_2$ at 423 K for 2.5 h (Table 2, entry 15). Gratifyingly, HMF conversion of 89.4% and BHMF selectivity of 86.2% were still achieved, which indicate that a crude HMF could be converted to BHMF by CTH process with a high yield to avoid an energy-intensive separation/purification of HMF. Namely, this CTH reaction system is a cost-efficient process for the practical production of BHMF from biomass-derived carbohydrates.

Recycling tests and characterizations of catalysts

Table 3 Recycling of the catalysts for the CTH of HMF to BHMF.[a]

Cycle	*X*, %	S_{BHMF}, %	S_{EMFA},%	S_{HMFDEA}, %
1	94.1	88.9	2.5	3.1
2	76.1	81.8	6.9	9.0
3	67.1	74.6	9.1	12.3
4	60.7	64.1	13.4	20.2
5	52.9	52.7	15.8	20.5
6[b]	74.9	63.2	19.8	17.0

[a] Reaction conditions: 1 g HMF, 1 g $ZrO(OH)_2$, 39 g ethanol, 423 k, 2.5 h, and N_2 at atmospheric conditions.
[b] The recovered catalyst used in the cycle 6 was regenerated by calcination at 573 K for 4 h after cycle 5.

The long-term stability and reusability of catalyst are of great importance for the practical production of BHMF to reduce the manufacturing cost. In a typical recycling test, the catalyst was separated from the reaction mixture by filtration after reaction, and then dried at 343 K for 2 h before reuse in the next cycle. As can be seen from Table 3, HMF conversion decreased considerably to 76.1% with a BHMF selectivity of 81.8% in the second cycle (Table 3, entry 2). Then, HMF conversion and BHMF selectivity gradually decrease to 52.9 and 52.7% if $ZrO(OH)_2$ was reused 5 times, and obvious increases of HMFDEA and EMFA selectivities were also observed (Table 3, entry 5). The partial deactivation of the spent catalyst was probably caused by carbon deposits during the reaction. Therefore, the spent $ZrO(OH)_2$ was regenerated by calcination at 573 K for 4 h to remove possible carbon deposits on the surface of catalyst, and HMF conversion and BHMF selectivity increased to 74.9% and 63.2% over this regenerated catalyst (Table 3, entry 6). The above finding indicated that the catalytic activity of the regenerated catalyst did not resume to the level of the fresh catalyst, and the regenerated catalyst still effectively promoted the etherification of BHMF with ethanol to form EMFA (Table 3, entry 6).

To gain more insights to the deactivation of spent and regenerated catalysts, we characterized these catalysts with XRD, SEM, FT-IR, CO_2-TPD, NH_3-TPD and elemental analysis.

XRD spectrums of the fresh, spent and regenerated catalyst show similar broad and weak peaks which indicate that the catalysts existed in amorphous form under the applied and regenerated conditions (Fig. 1). Meanwhile, as shown in SEM images, the size of the aggregations of the primary crystallites and the surface morphology of these catalysts don't change evidently before and after use (Fig. 2). However, the diameter of primary crystallites in regenerated catalysts increased remarkably.

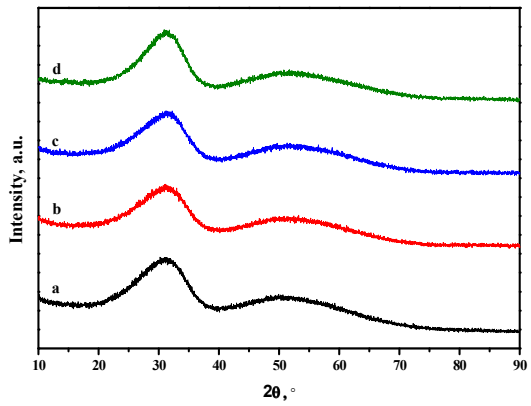

Fig. 1 XRD patterns for the fresh catalyst (a), the spent catalyst after the first cycle (b), the spent catalyst after the fifth cycle (c) and the regenerated catalyst by calcination at 573 K for 4 h after cycle 5 (d).

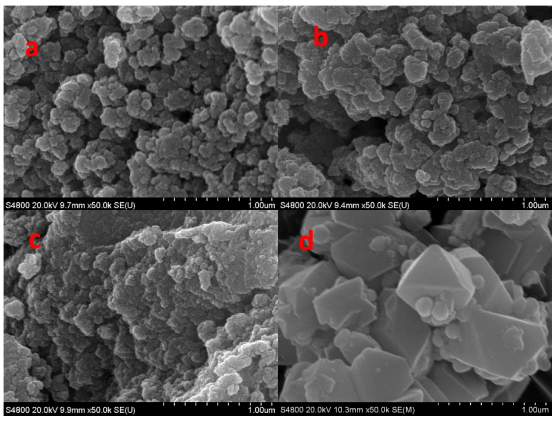

Fig. 2 SEM images for the fresh catalyst (a), the spent catalyst after the first cycle (b), the spent catalyst after the fifth cycle (c) and the regenerated catalyst by calcination at 573 K for 4 h after cycle 5 (d).

Table 4 Elemental analysis and BET surface areas for the fresh, spent and regenerated catalyst.

Entry	Recycle times	Carbon Residues (wt%)	Hydrogen Content (wt%)	S_{BET} (m^2/g)
1	Fresh	0.6	2.2	345.7
2	1	7.1	1.8	241.9
3	5	9.5	1.6	162.8
4	Regenerated	1.0	1.1	237.0

Compared with the fresh catalyst, the surface area of the spent catalyst was decreased significantly from 324.7 m^2/g to 241.9 m^2/g after the first use and to 162.8 m^2/g after the fifth use (Table 4, entries 1-3). In addition, the carbon residues of the spent catalyst increased to 7.1 wt% after the first use (Table 4, entry 2), which was probably responsible for the drop in the specific surface area and the deactivation of the spent catalyst. The carbon residues of the catalyst further increased to 9.5 wt% after the fifth run, and a remarkable decrease in the specific surface area was also observed. Moreover, the specific surface area of the regenerated catalyst increased to 237.0 m^2/g after calcination at 573 K for 4 h, and the carbon residues decreased considerably to 1.0 wt% compared to the spent catalyst after the fifth use.

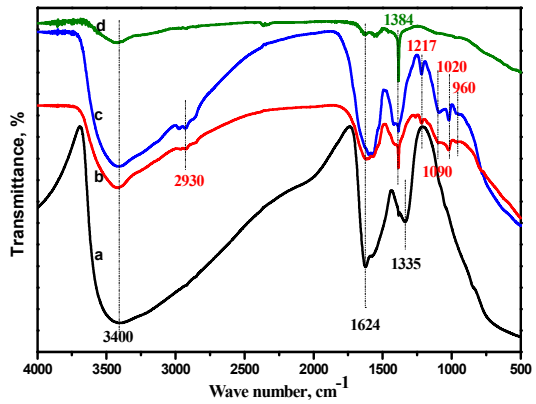

Fig. 3 FI-IR patterns for the fresh catalyst (a), the spent catalyst after the first cycle (b), the spent catalyst after the fifth cycle (c) and the regenerated catalyst by calcination at 573 K for 4 h after cycle 5 (d).

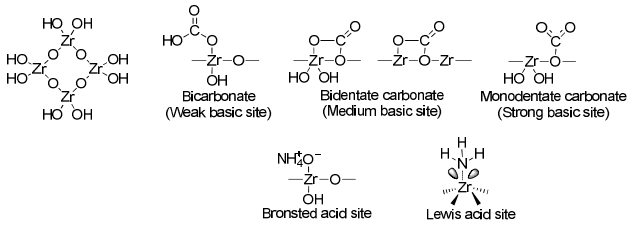

Scheme 2 Model structure of $ZrO(OH)_2$, the types of the interactions of CO_2 on the surface of $ZrO(OH)_2$ and ZrO_2 and acid sites on the surface of $ZrO(OH)_2$

As shown in the FT-IR patterns, the broad band at 3400 cm^{-1} is due to the stretching vibration of the hydroxyl in the zirconium hydroxide. The band at 1624 cm^{-1} may be attributed to the scissor bending mode of molecular water, and to O–C–O

stretching modes of CO_2 interacted with terminal OH groups of zirconium hydroxide (Scheme 2). [37] The band at 1340 cm^{-1} of the fresh catalyst was assigned to bidentate carbonates which was medium basic site and the band at 1384 cm^{-1} of the other catalysts was assigned to monodentate carbonate which was strong basic site shown in Scheme 2. [38-40] Compared to the other catalysts, the band at 1624 cm^{-1} of the regenerated catalyst was unconspicuous, which indicated that the OH groups were removed in the calcination process and chemical structure of the regenerated catalyst was speculated to be ZrO_2. This observation may explain the phenomena that the catalytic reactivity of the catalyst did not completely recover after regeneration by calcination (Table 3, entry 6), although the carbon residues of the spent catalyst could be removed by calcination (Table 4, entry 4).

Compared to the fresh catalyst, new absorption peaks of the spent catalysts appeared at about 2930, 1217, 1090, 1020 cm^{-1}, probably resulted from the above-mentioned carbon residues as shown in Table 6, which may responsible for the deactivation of the catalyst. For instance, the broad band at 2930 cm^{-1} is representative of the stretching vibration of C–H of alkane. The broad band at 1217 and 1090 cm^{-1} is attributed to of the bending vibration of O-H and the stretching vibration of C-O of alcohol, respectively. Moreover, IR peaks centered at 1020 and 960 cm^{-1} is assigned to the stretching vibration of C-O-C.

To gain more insights about the acid-base properties of the catalyst, CO_2-TPD and NH_3-TPD measurements were performed and the results were presented in Fig. 4 and Fig. 5, respectively. There were two significant desorption peaks at 381 K and 457 K in the CO_2-TPD profile of the fresh catalyst, which could be assigned to the weak basic sites and the medium basic sites on which CO_2 was absorbed in the form of bicarbonate and bidentate carbonate, as shown in Scheme 2 [41]. As for the spent catalysts, a broad desorption peak at around 636 K assigned to strong basic sites was detected, and the weak and medium basic sties were much fewer comparing to the fresh catalyst. However, only strong basic sites with a significant desorption peak centered at 700 K was detected in the regenerated catalyst. There results were in line with the FI-IR characterization. Similarly, a broad desorption peak assigned to the Lewis acid sites was observed at 627 K in NH_3-TPD profiles for both spent and regenerated catalysts. However, Bronsted acid sites at 453 K was not detected, which was significant in the profiles of the fresh catalyst. [37]

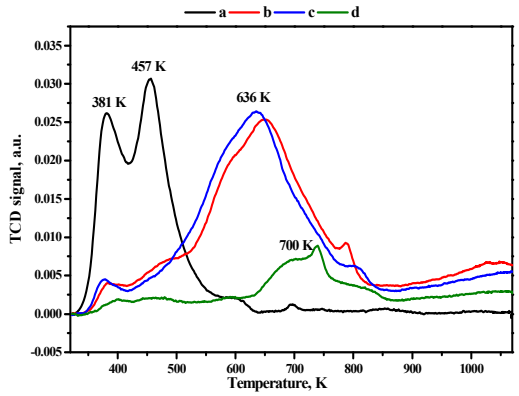

Fig. 4 CO_2-TPD profiles for the fresh catalyst (a), the spent catalyst after the first cycle (b), the spent catalyst after the fifth cycle (c) and the regenerated catalyst by calcination at 573 K for 4 h after cycle 5 (d).

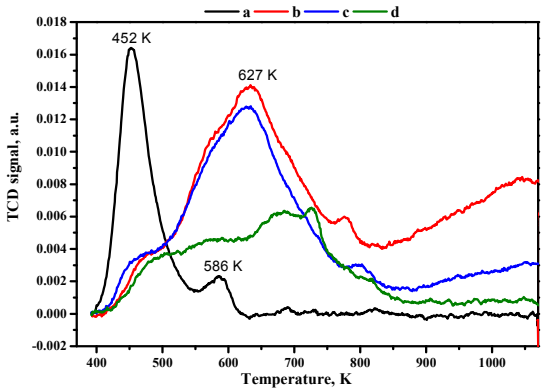

Fig. 5 NH_3-TPD profiles for the fresh catalyst (a), the spent catalyst after the first cycle (b), the spent catalyst after the fifth cycle (c) and the regenerated catalyst by calcination at 573 K for 4 h after cycle 5 (d).

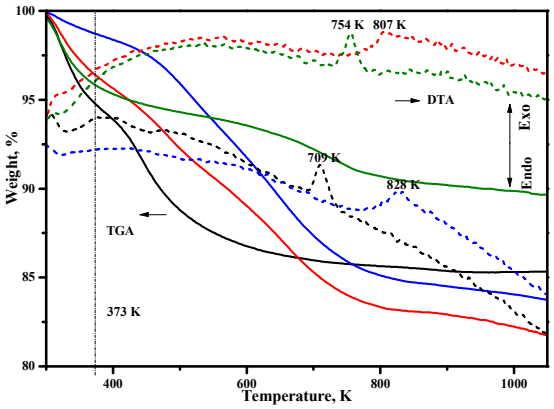

Fig. 6 TGA-DTA profiles for the fresh catalyst (black), the spent catalyst after the first cycle (red), the spent catalyst after the fifth cycle (blue) and the regenerated catalyst by calcination at 573 K for 4 h after cycle 5 (olive).

In addition, the thermogravimetric analysis of the catalysts was conducted. As indicated in Fig. 4, the fresh catalyst absorbed more water than the spent catalyst and the regenerated catalyst because more weight loss of the former before 373 K was observed compared to the latter, which probably owing to the relatively high the specific surface of the fresh catalyst (Table 4, entry 1). Nevertheless, if the temperature increased subsequently to 1073 K, the weight loss of the spent catalyst after the fifth cycle was reached 15.1 wt%, which was higher than the weight loss of the fresh catalyst (9.6 wt%). Carbon deposits absorbed on the spent catalyst surface led to this higher weight loss which is in accordance with the results of elemental analysis (Table 4). Simultaneously, the weight loss of the regenerated catalyst was only 6.23 wt% that is less than that of the fresh catalyst, probably due to the removal of OH groups during the regeneration by calcination. Meanwhile, the exothermic peaks with a continuous weight loss appeared around 709, 754, 807, 828 K were observed, which were attributed to the enthalpy of the transformation of the amorphous zirconia into the crystalline zirconia, accompanying by the release of hydroxyl groups of remaining Zr–OH species in the incomplete ZrO_2 lattice. [43] The delay of the crystal transition of the spent catalyst probably was caused by carbon deposits.

Reaction mechanism

In order to gain more insight to the mechanism for the CTH of HMF via MPV reduction, poisoning experiments were also carried out by introducing extra additives into the reaction system and the results are showed in Table 5. In the presence of N_2 (10 Bar) at the beginning of reaction (Table 5, entry 2), both the HMF conversion and BHMF yield were slightly decreased, which indicated the extra pressure was not beneficial to the reaction. H_2 and O_2 (Table 5, entries 3 and 4) as additive was introduced to the reaction respectively to prove the existence of H^-, because hydride transfer was generally believed to be responsible for the MPV reduction [28]. As entry 3 showed, when H_2 was as added, the conversion of HMF and selectivity to BHMF was unchanged. While O_2 was charged, the conversion of HMF decreased to75.0% with a significantly drop in BHMF selectivity to 1.7% (Table 5, entry 4). It is noted that the oxygen pressure was dropped to 4 bar after reaction, and water content was measured as 4.41 wt%, whereas only 1.26 wt% water was measured in the absence of oxygen. Simultaneously, compounds of **1** and **2** (Scheme 1) were detected by GC-MS in the reaction solution with O_2 as additive resulting in a significantly drop in BHMF selectivity, which were generated via aldol condensation between HMF and aldehyde. These results implied that oxygen competed with HMF to capture H^- and coverted to water subsequently, which promoted aldol condensation of HMF with aldehyde and suppressed the transfer hydrogenation of HMF to BHMF. Namely, H^- play an important role in the MPV reaction rather than molecule hydrogen. Meanwhile, the addition of water to reaction system was probably contributed to the catalyst disabled, which led to the drop in both HMF conversion and BHMF selectivity (Table 5, entry 5 and 6).

Table 5 Effect of additives on the CTH of HMF in ethanol over $ZrO(OH)_2$ [a]

Entry	Additives	*X*, %	S_{BHMF}, %	S_{EMFA},%	S_{HMFDEA}, %
1	no	94.1 (1.26)[c]	88.9	1.8	1.0
2	10 bar N_2	91.9	79.1	11.9	2.3
3	10 bar H_2	92.1	84.9	5.3	3.0
4	10 bar O_2	75.0 (4.41)[c]	1.7	11.8[d]	13.1[f]
5	2.5wt% H_2O	64.5	88.1	4.8	1.0
6	5wt% H_2O	60.0	85.5	7.2	1.3
7	Benzoic acid[b]	31.4	51.7	4.6	-
8	Pyridine[b]	87.1	90.1	1.2	2.0

[a] Reaction conditions: 1 g HMF, 1 g $ZrO(OH)_2$, 39 g ethanol, 423 k, 2.5 h, N_2 at atmospheric conditions.
[b] 0.5 g additive was introduced
[c] Moisture content of the solution after reaction, wt%
[d] the selectivity of BEMF
[f] the selectivity of EMFDEA

In line of the results of the entry 7 (Table 5), the addition of benzoic acid drastically reduced the conversion of HMF and the catalyst was almost total disabled, indicating that catalytic activity was closely related to basic sites on the catalyst surface. [40] However, in the presence of pyridine (Table 5, entry 8), the catalytic activity of $ZrO(OH)_2$ was slightly decreased. The pyridine adsorbed on the surface of the catalyst led to the weak poisoning effect. Meanwhile, an increase of BHMF and a drop of EMFA was obtained, which illustrated that the pyridine was adsorbed on Lewis acid sits of the catalyst and inhibited etherification of BHMF to EMFA. Combined with characterization of the catalysts discussed above, along with the OH group which contributed to weak basic sites (Scheme 2) removed in the recycling and calcination process, more Zr-O formation and the amount of Lewis acid sits enhancement were occurred, [39] accelerating the etherification resulting in a drop of BHMF selectivity and an increase of EMFA, in line with the results of recycling tests (Table 3).

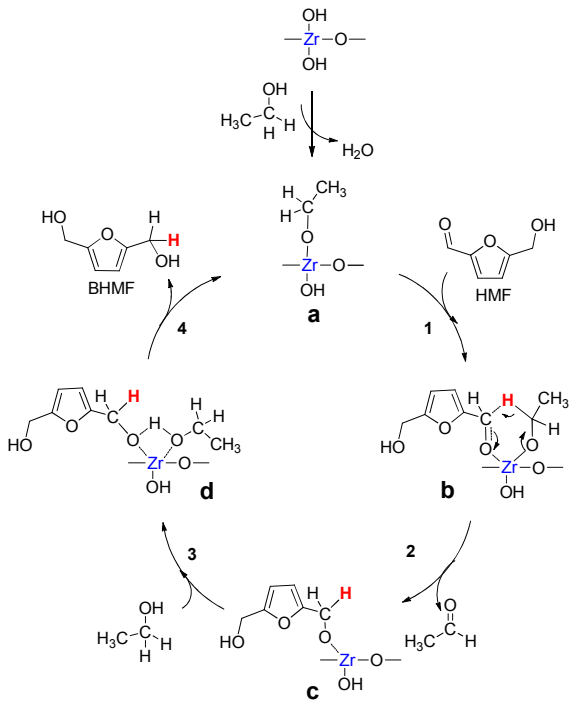

Scheme 3 Proposed mechanism for the CTH of HMF to BHMF over $ZrO(OH)_2$

In light of the above mentioned observation and in combination with the results of characterization for the fresh, spent and regenerated catalyst, the OH group of $ZrO(OH)_2$ was suggested to be important during the reaction process and proposed to act as sites for ligand exchange with ethanol to form zirconium ethoxide **a** (Scheme 3). [42] Based on these results, a classic catalytic cycle involving six-membered ring transition state over $ZrO(OH)_2$ for the CTH from HMF to BHMF via MPV reduction was proposed in the scheme 3. In the key step, the carbonyl oxygen of HMF coordinated with the alkoxide **a** to form a six-membered ring transition state **b** on the zirconium metal center. In intermediates **b**, the hydride was transferred from the alkoxide to the carbonyl of HMF by the concerted process of a six-membered ring-like structure. At this point the new carbonyl (aldehyde) dissociated and gave off the intermediate species **c** and then another ethanol from solution coordinated to it to form species **d**. Finally, the newly reduced carbonyl (BHMF) dissociated to regenerate the alkoxide **a**.

Conclusions

In summary, an efficient and simple CTH system for synthesis of BHMF from biomass-derived HMF via MPV reduction was developed, in which easy-stored ethanol was employed as the hydrogen donor and solvent simultaneously and inexpensive and active $ZrO(OH)_2$ was used as catalyst. More importantly, this reaction system was also effective for the crude HMF produced from biomass-derived carbohydrates without purification. Combination with the results of characterization for the catalysts and poisoning experiments, the OH group was found to be important to MPV reaction.

Experimental

Materials

HMF was purchased from Shanghai Energy Chemical Industrial Co. Ltd. (Shanghai, China). Standard BHMF was supplied by BePharm Co. Ltd. (Shanghai, China). $ZrOCl_2$ was obtained from Aladdin Reagent Co. Ltd. (Shanghai, China). Other reagents and chemicals were all of analytical grade from Sinopharm Chemical Reagent Company Co. Ltd. (Shanghai, China) and used without further purification.

Catalysts preparation

All metal hydroxides were prepared by precipitation method using their chloride salts as the precursors. The detailed preparation procedure of $ZrO(OH)_2$ was as follows: $ZrOCl_2{\cdot}8H_2O$ was dissolved in de-ionized water to prepare a 100 g/L $ZrOCl_2$ aqueous solution. Concentrated NH_4OH was added to the resulting solution to adjust the pH value between 9 and 10 with vigorous stirring, and then aged for 24 h at room temperature. The obtained precipitate was washed thoroughly with de-ionized water until the chloride ion in the filtrate could not be identified and was dried at 383 K for 12 h. The dried precipitate was powdered below 100-mesh.

Catalyst Characterization

X-ray diffraction (XRD) patterns of the catalysts were carried out by using an Ultima IV Advance X-ray diffractometer with CuKα radiation source operated at 40 kV and 40 mA. Data was collected from 2θ between 10° and 90° with a step of 0.02° at a scanning speed of 10°/min. FT-IR spectrums were recorded on a Varian 3100 FT-IR spectrometer. SEM images were performed on a Hitachi S-4800 suing 20 kV. Thermal gravimetric analysis and differential thermal gravimetric analysis (TGA/DTG) were carried out on a SDT Q600 thermal analyzer under a dynamic N_2 atmosphere (100 mL/min) at the temperature range of 293-1073 K with a heating rate of 10 K/min. BET surface areas were measured by N_2 adsorption-desorption isotherms at liquid nitrogen temperature on a ASAP 2020 HD 88 surface area and porosimetry analyzer (Micromeritics), the samples degassed at 373 K for 4 h in a vacuum before N_2 adsorption. Elemental analysis was performed by an Elementar Vario EL III (Elementar Analysensysteme GmbH, Germany). CO_2 temperature-programmed desorption (CO_2-TPD) and NH_3 temperature-programmed desorption (NH_3-TPD) were carried out with a Micromeritics AutoChem II Chemicsorption Analyzer 2920, which was connected to a thermal conductivity detector. Typically, the the sample (30 mg) loaded into the quartz tube was first pretreated at a rate of 20 K/min up to 393 K in a He gas flow for 30 min to remove species adsorbed on the surface. The adsorption of CO_2 was performed at 323 K in a CO_2–He (10 vol% CO_2) mixture for 30 min, and then the remaining and weakly adsorbed CO_2 was purged with high-purity He. TPD was

performed in the He flow by raising the temperature to 1073 K at a rate of 20 K/min and then keeping it at 1073 K for 30 min. The desorbed CO_2 was detected by the mass spectrometer. NH_3-TPD was performed by using a similar procedure.

Typical procedure for the production of BHMF

The experiments were carried out in a 100 ml cylindrical stainless steel pressurized reactor made by PARR instrument company, USA. In a typical reaction, HMF (1 g), solvent (39 g), and catalyst (0.5 g) were mixed to form a suspension and poured into the reactor. The reactor was purged with N_2 five times at atmospheric conditions and then brought to the desired temperature by external heating with stirring at 600 rpm. After running the reaction for a desired duration, the reactor was taken from the stove and cooled to room temperature. The liquid product and solid acid catalyst were separated by filtration.

After evaporating the ethanol from the liquid product, the crude solid mixture was obtained and then purified by column chromatography on silica gel with a chloroform/methanol mixture afforded BHMF as an off-white solid. ^{1}H NMR: δ 6.23 (2H), 4.70 (2H), 4.43 (4H); ^{13C} NMR: δ 153.68, 109.09, 55.85, shown in Fig. S11-12.

Products analysis

The qualitative analysis of sample was determined on a GC-MS (Thermo Trace 1300 and ISQ LT) instrument equipped with TR-5MS column of 15 m × 0.25 mm × 0.25 μm and electron impact ionization (EI).

HMF, BHMF and other products in the reaction mixture was analyzed by using an Agilent 7890 series with a DB-WAXETR column (30 m × 0.25 mm × 0.25 μm) and a flame ionization detector (FID) operating at 543 K. The carrier gas was N_2 with a flow rate of 1.0 ml/min. The following temperature program was used in the analysis: 313 K (4 min)-5 K/min-373 K-10 K/min-633 K (2 min). The amount of HMF in the reaction products was determined using a calibration curves obtained by analyzing standard solutions with known amount. The FID sensitivities for compounds HMFDEA, EMFDEA, EMFA, and BEMF were assumed to be equal to that for BHMF. HMF conversion (X, %), BHMF yield (Y_{BHMF}, %), and BHMF selectivity (S_{BHMF}, %) were calculated according to Equations (1)-(3):

$$\text{HMF conversion} = (1 - \frac{\text{Mole of HMF in the products}}{\text{Initial mole of HMF}}) \times 100\%$$

$$\text{DHMF yield} = \frac{\text{Mole of DHMF in the products}}{\text{Innitial mole of HMF}} \times 100\%$$

$$\text{DHMF selectivity} = \frac{\text{Mole of DHMF in the products}}{\text{Innitial mole of HMF-Mole of HMF in the products}} \times 100\%$$

Acknowledgements

This work was financially supported by the Key Program for Cooperation between Universities and Enterprises in Fujian Province (No.2013N5011), the Key Research Program from Science and Technology Bureau of Xiamen City, China (No.3502Z20131016), and Natural Science Foundation of Fujian Proince, China (No.2015J05034).

Notes and references

1 E. L. Kunkes, D. A. Simonetti, R. M. West, J. C. Serrano-Ruiz, C. A.Garter and J. A. Dumesic, *Science*, 2008, **322**, 417-421.
2 G. W. Huber, J. N. Chheda, Christopher J. Barrett and J. A. Dumesic, *Science*, 2005, **308**, 1446-1450.
3 M. J. Climent, A. Corma and S. Iborra, *Green Chem.*, 2014, **16**, 516.
4 L. Hu, G. Zhao, W. Hao, X. Tang, Y. Sun, L. Lin and S. Liu, *RSC Adv.*, 2012, **2**, 11184-11206.
5 Á. Szabolcs, M. Molnár, G. Dibó and L. T. Mika, *Green Chem.*, 2013, **15**, 439.
6 S. W. Fizpatrick*, US Pat.,* US005608105A, 1997.
7 K. Yan, G. Wu, T. Lafleur and C. Jarvis, *Renewable and Sustainable Energy Rev.*, 2014, **38**, 663-676.
8 X. Tang, X. Zeng, Z. Li, L. Hu, Y. Sun, S. Liu, T. Lei and L. Lin, *Renewable Sustainable Energy Rev.*, 2014, **40**, 608-620.
9 A. Corma, S. Iborra and A. Velty, *Chem. Rev.*, 2007, **107**.
10 G. W. Huber, S. Iborra and A. Corma, *Chem. Rev.*, 2006, **106**, 4044-4098.
11 L. Hu, L. Lin and S. Liu, *Ind. Eng. Chem. Res.*, 2014, **53**, 9969-9978.
12 O. Casanova, S. Iborra and A. Corma, *ChemSusChem*, 2009, **2**, 1138-1144.
13 O. Casanova, S. Iborra and A. Corma, *J. Catal.*, 2009, **265**, 109-116.
14 Z.-Z. Yang, J. Deng, T. Pan, Q.-X. Guo and Y. Fu, *Green Chem.*, 2012, **14**, 2986.
15 J. Ma, Z. Du, J. Xu, Q. Chu and Y. Pang, *ChemSusChem*, 2011, **4**, 51-54.
16 W. J. Pentz*, US Pat.,* 4426460, 1984.
17 A. Gandini, ACS Symposium series-American Chemical Society, 1990, 197-208.
18 J. M. Timko and D. J. Cram, *J. Am. Chem. Soc.*, 1974, **96**, 7159-7160.
19 H. Cai, C. Li, A. Wang and T. Zhang, *Catal. Today*, 2014, **234**, 59-65.
20 A. S. Amarasekara and B. Wiredu, *Ind. Eng. Chem. Res.*, 2015, **54**, 824-831.
21 R. Alamillo, M. Tucker, M. Chia, Y. Pagán-Torres and J. Dumesic, *Green Chem.*, 2012, **14**, 1413.
22 M. Chatterjee, T. Ishizaka and H. Kawanami, *Green Chem.*, 2014, **16**, 1543.
23 E.-S. Kang, D. W. Chae, B. Kim and Y. G. Kim, *J. Ind. Eng. Chem.*, 2012, **18**, 174-177.
24 S. Subbiah, S. P. Simeonov, J. M. S. S. Esperança, L. P. N. Rebelo and C. A. M. Afonso, *Green Chem.*, 2013, **15**, 2849.
25 T. Pasini, G. Solinas, V. Zanotti, S. Albonetti, F. Cavani, A. Vaccari, A. Mazzanti, S. Ranieri and R. Mazzoni, *Dalton Trans.*, 2014, **43**, 10224-10234.
26 J. Jae, W. Zheng, R. F. Romn-Leshkov and D. G. Vlachos, *ChemSusChem*, 2013, **6**, 1158-1162.
27 X. Tang, X. Zeng, Z. Li, W. Li, Y. Jiang, L. Hu, S. Liu, Y. Sun and L. Lin, *ChemCatChem*, 2015, **7**, 1372–1379.
28 X. Tang, H. Chen, L. Hu, W. Hao, Y. Sun, X. Zeng, L. Lin and S. Liu, *Appl. Catal., B*, 2014, **147**, 827-834.
29 T. S. Hansen, K. Barta, P. T. Anastas, P. C. Ford and A. Riisager, *Green Chem.*, 2012, **14**, 2457.
30 X. Tang, Z. Li, X. Zeng, Y. Jiang, S. Liu, T. Lei, Y. Sun and L. Lin, *ChemSusChem*, 2015, **8**, 1601-1607.
31 T. D. Matson, K. Barta, A. V. Iretskii and P. C. Ford, *J. Am. Chem. Soc.*, 2011, **133**, 14090-14097.

32 J. Zaldivar, J. Nielsen and L. Olsson, *Appl. Microbiol. Biotechnol.*, 2001, **56**, 17-34.
33 J. G. Jakobsen, T. L. Jørgensen, I. Chorkendorff and J. Sehested, *Appl. Catal., A*, 2010, **377**, 158-166.
34 M. Balakrishnan, E. R. Sacia and A. T. Bell, *Green Chem.*, 2012, **14**, 1626.
35 J. D. Lewis, S. Van de Vyver, A. J. Crisci, W. R. Gunther, V. K. Michaelis, R. G. Griffin and Y. Roman-Leshkov, *ChemSusChem*, 2014, **7**, 2255-2265.
36 J. Yang, K. De Oliveira Vigier, Y. Gu and F. Jerome, *ChemSusChem*, 2015, **8**, 269-274.
37 W. Hertl, *Langmuir*, 1989, **5**, 96-100.
38 G. Y. Guo and Y. L. Chen, *J. Mater. Sci.*, 2004, **39**, 4039-4043.
39 T. Yamaguchi, *Catal. Today*, 1994, 199-218.
40 V. A. Ivanov, F. A. Bachelier and J. C. Lavalley, *J. Mol. Catal.*, 1994, **91**, 46-59.
41 B. Bachiller-Baeza, I. Rodriguez-Ramos and A. Guerrero-Ruiz, *Langmuir*, 1998, **14**, 3556-3564.
42 S. H. Liu, S. Jaenicke and G. K. Chuah, *J. Catal.*, 2002, **206**, 321-330.
43 P. Manivasakan, V. Rajendran, P. Ranjan Rauta, B. Bandhu Sahu and B. Krushna Panda, *J. Am. Ceram. Soc.*, 2011, **94**, 1410-1420.